

Analyst

Accepted Manuscript



This is an *Accepted Manuscript*, which has been through the Royal Society of Chemistry peer review process and has been accepted for publication.

Accepted Manuscripts are published online shortly after acceptance, before technical editing, formatting and proof reading. Using this free service, authors can make their results available to the community, in citable form, before we publish the edited article. We will replace this *Accepted Manuscript* with the edited and formatted *Advance Article* as soon as it is available.

You can find more information about *Accepted Manuscripts* in the [Information for Authors](#).

Please note that technical editing may introduce minor changes to the text and/or graphics, which may alter content. The journal's standard [Terms & Conditions](#) and the [Ethical guidelines](#) still apply. In no event shall the Royal Society of Chemistry be held responsible for any errors or omissions in this *Accepted Manuscript* or any consequences arising from the use of any information it contains.

1
2
3 **Polarity Switching Mass Spectrometry Imaging of Healthy and Cancerous Hen Ovarian Tissue Sections**
4 **by Infrared Matrix-Assisted Laser Desorption Electrospray Ionization (IR-MALDESI)**
5
6
7

8 Milad Nazari and David C. Muddiman*
9

10
11
12 *W. M. Keck FTMS Laboratory for Human Health Research, Department of Chemistry,*
13
14 *North Carolina State University, Raleigh, NC 27695*
15
16
17
18
19
20
21
22
23
24
25
26
27
28
29
30
31
32
33
34

35 **Keywords:** Mass Spectrometry Imaging, IR-MALDESI, Tissue Analysis, Lipids, Ovarian Cancer, Hen Model,
36 Lipid Metabolism, Polarity Switching
37
38
39
40
41
42
43

44 ***Author for Correspondence**

45 David C. Muddiman, Ph.D.
46 W. M. Keck FTMS Laboratory for Human Health Research
47 Department of Chemistry
48 North Carolina State University
49 Raleigh, North Carolina 27695
50 Phone: 919-513-0084
51 Email: david_muddiman@ncsu.edu
52
53
54
55
56
57
58
59
60

Abstract

Mass spectrometry imaging (MSI) is a rapidly evolving field for monitoring the spatial distribution and abundance of analytes in biological tissue sections. It allows for direct and simultaneous analysis of hundreds of different compounds in a label-free manner. In order to obtain a comprehensive metabolite and lipid data, a polarity switching MSI method using infrared matrix assisted laser desorption electrospray ionization (IR-MALDESI) was developed and optimized where the electrospray polarity was alternated from one voxel to the next. Healthy and cancerous ovarian hen tissue sections were analyzed using this method. Distribution and relative abundance of different metabolites and lipids within each tissue section were discerned, and differences between the two were revealed. Additionally, the utility of using mass spectrometry concepts such as spectral accuracy and sulfur counting for confident identification of analytes in an untargeted method are discussed.

Introduction

The advent of “soft” ionization methods such as electrospray ionization (ESI)¹ and matrix-assisted laser desorption/ionization (MALDI)^{2,3} over two decades ago helped mass spectrometry (MS) evolve into an indispensable tool for analyzing biological samples.⁴ Mass spectrometry has been used extensively in cancer research for discovery of novel disease biomarkers and also as a cancer diagnostic and imaging tool.⁵⁻⁷ One of the rapidly evolving fields in MS-based cancer research is mass spectrometry imaging (MSI). In MSI experiments, materials are desorbed directly from tissues, ionized, and sampled by a mass spectrometer. At the same time, the exact location where the tissue-related material was desorbed from is also recorded. The mass spectra along with the locations they were collected from are used to generate heat maps showing relative abundance and distribution of analyte(s) of interest within a tissue section.

The sensitivity and specificity of MS coupled with the label-free nature of imaging have helped MSI become an attractive tool in cancer research for identifying diagnostic biomarkers for early

1
2
3 detection of cancer and visualizing tumor margins in cancerous tissues.⁸⁻¹¹ The most common ionization
4 method for MSI analyses is MALDI; however, MALDI MSI suffers from drawbacks associated with its
5 requirements for high vacuum and a need for an organic acid matrix.¹² Furthermore, MALDI relies on
6 partitioning of analytes into the matrix crystals, which may be variable across different tissues types.¹³ In
7 order to circumvent these limitations, numerous ionization methods such as atmospheric pressure
8 MALDI (AP-MALDI)¹⁴, desorption electrospray ionization (DESI)¹⁵, and matrix-assisted laser desorption
9 electrospray ionization (MALDESI)¹⁶ have been developed for MSI at atmospheric pressure. The recent
10 advances in atmospheric pressure MSI were the subject of a recent review.¹⁷

11
12
13
14
15
16
17
18
19
20
21
22 MALDESI was the first ionization method combining resonant matrix-assisted laser desorption
23 with electrospray post-ionization.¹⁶ In MALDESI experiments, a laser (UV or IR) is used to resonantly
24 excite an endogenous or exogenous matrix in order to desorb material within the focal volume of the
25 laser. MSI of biological tissue sections using MALDESI is performed using a mid-infrared (IR) laser, where
26 a thin layer of ice is used as the energy-absorbing matrix.¹⁸ The O-H stretching modes of water present
27 in the tissue and the ice layer are resonantly excited by absorbing the energy of a mid-IR ($\lambda = 2940$ nm)
28 laser pulse, facilitating the desorption of neutral material from the tissue section. The plume of
29 desorbed neutrals partitions into the charged droplets of an orthogonal electrospray, and are ionized in
30 an ESI-like mechanism.¹⁶ Using ice as an exogenous matrix accounts for variations in the water content
31 in different tissue compartments, and has been shown to greatly improve desorption and the resulting
32 ion abundances.^{18,19} Additionally, the matrix-related peaks observed in lower m/z regions in MALDI MSI
33 are eliminated.

34
35
36
37
38
39
40
41
42
43
44
45
46
47
48
49 One of the applications of IR-MALDESI MSI is in the field of lipidomics. Lipids are family of
50 naturally occurring biomolecules, ubiquitous across all living cells, and second only to proteins in
51 abundance.²⁰ Lipid profiles provide valuable information for understanding the biological basis of many
52 disease. Alterations in lipid metabolism have been linked to several diseases such as hypertension,
53
54
55
56
57
58
59
60

1
2
3 diabetes, and cancer.^{21,22} Most lipid classes consist of a polar headgroup and a non-polar hydrocarbon
4 tail. Differences in the composition of the headgroup, along with variations in the length and saturation
5
6 of the hydrocarbon tail result in a remarkable diversity in molecular structures of lipids. The differences
7
8 in the headgroup can also lead to significant differences in ionization efficiency of different lipid classes.
9
10 For instance, lipids with positively charged headgroups such as phosphatidylcholines (PC) and
11
12 sphingomyelins (SM) are readily detected in positive-ion mode, whereas other lipid classes such as
13
14 glycerophosphoinositols (PI) ionize more efficiently in negative-ion mode.²³ Therefore, analyzing tissue
15
16 sections in both polarities is essential to obtaining data representative of all lipids. Two MSI
17
18 experiments, one in each polarity, could be used at the cost of time and sample. IR-MALDESI MSI using
19
20 polarity switching affords the same biochemical information, while shortening the data acquisition time
21
22 drastically and allowing all measurement to be made from the same tissue section. To this end, a
23
24 polarity switching MSI method was developed where adjacent voxels were analyzed with opposing
25
26 polarities. Using this method, the distribution and relative abundance of lipids and other metabolites
27
28 can be simultaneously monitored in an untargeted fashion, and a list of candidates for targeted analyses
29
30 can be generated. In order to evaluate the utility of the polarity switching MSI for screening alterations
31
32 in lipid metabolism in cancer tissues, the hen model for ovarian cancer (OVC)²⁴⁻²⁶ was selected for
33
34 untargeted lipid analysis.
35
36
37
38
39
40
41

42 OVC is the fifth leading cause of cancer deaths in women in the United States, and is the most
43
44 lethal of gynecologic cancers.²⁷ Despite advancements in medical care for ovarian cancer patients,
45
46 median survival length for these patients is approximately 40 months²⁸, and mortality rates have
47
48 remained relatively constant over the past 30 years due to lack of reliable biomarkers for early
49
50 diagnosis.^{29,30} Many animal models, including the hen³¹, mouse³², and rat³³ have been developed in
51
52 order to understand the processes involved in initiation and progression of OVC and control the
53
54 subjects' environment. The domestic egg laying hen is the only non-human animal model for
55
56
57
58
59
60

1
2
3 spontaneous development of OVC with a high prevalence.^{31,34,35} The OVC in hen is also histologically
4 similar to that in women³⁶, and its prevalence increases with age.³⁷ Additionally, in both cases the cancer
5 metastasizes to similar tissues with an accumulation of ascites fluid.³¹
6
7
8
9

10 Applications of MSI in OVC research are nascent, with most efforts focusing on protein
11 expression.³⁸⁻⁴¹ However, numerous reports of alterations in lipid metabolism have been reported in
12 OVC patients.⁴²⁻⁴⁵ Herein, we present a report of polarity switching MSI performed at atmospheric
13 pressure using IR-MALDESI and its application in untargeted screening of lipids and other metabolites in
14 healthy and cancerous hen ovarian tissues. Spatial distribution and relative abundance of more than 700
15 metabolites were simultaneously monitored, and differences between the two tissues were discerned.
16
17
18
19
20
21
22
23

24 **Experimental**

25 *Materials*

26 HPLC-grade methanol and water were purchased from Burdick and Jackson (Muskegon, MI,
27 USA). Acetic acid, ammonium hydroxide, ammonium acetate, and 2,2,2-trifluoroethanol (TFE) were
28 purchased from Sigma-Aldrich (St. Louis, MO, USA), and were used without any purification. Nitrogen
29 gas (purity $\geq 99.999\%$) used for purging the MALDESI imaging enclosure was obtained from Arc3 Gases
30 (Raleigh, NC, USA).
31
32
33
34
35
36
37
38
39
40

41 *Samples*

42 Ovarian tissues were obtained from age-matched healthy and cancerous C-strain white leghorn
43 commercial egg laying hens. Birds were managed in accordance with the Institute for Laboratory Animal
44 Research Guide, and all husbandry practices were approved by North Carolina State University
45 Institutional Animal Care and Use Committee (IACUC). Tissues were flash frozen in isopentane chilled in
46 a liquid nitrogen bath, and stored at $-80\text{ }^{\circ}\text{C}$ until the time of the experiment. The tissues were sectioned
47 into $10\text{-}\mu\text{m}$ -thick sections at $-20\text{ }^{\circ}\text{C}$ using a Leica CM1950 cryostat (Buffalo Grove, IL, USA). The tissue
48 sections were thaw mounted onto pre-cleaned glass microscope slides, and were analyzed right away.
49
50
51
52
53
54
55
56
57
58
59
60

IR-MALDESI Imaging Source Coupled to Q Exactive Plus

The details of the IR-MALDESI source design and implementation have been described elsewhere in detail.^{18,46} In summary, the tissue section mounted on a glass slide is placed on a water-cooled Peltier plate, which is mounted on a computer controlled XY motion stage and housed within a custom-built enclosure. The plate is cooled to -10 °C after the enclosure is purged with dry nitrogen in order to reduce the relative humidity (RH) to <5%. After the tissue section has reached thermal equilibrium (~10 minutes), the sample is then exposed to the laboratory ambient RH by opening the enclosure, and a thin layer of ice is deposited on the surface of the tissue section due to desublimation of water from the air. Once the ice layer is formed, the enclosure is purged with dry nitrogen in order to maintain the RH at ~10%, which has been found to maintain a consistent ice matrix layer throughout the experiment.¹⁸ A mid-IR laser (IR Opolette 2371, OPOTEK, Carlsbad, CA, USA) operated at a wavelength of 2940 nm is then used to resonantly excite the O-H stretching mode of water molecules present in biological tissue and exogenous ice layer, facilitating the desorption of neutral molecules from the tissue. The desorbed neutrals then partition into charged droplets of an orthogonal electrospray, and are ionized in an ESI-like fashion.¹⁶ Different modifiers at various concentrations (20 mM ammonium hydroxide, 5 mM ammonium acetate, 1 mM acetic acid, and 100 mM TFE) were added to a 50/50 (v/v) solution of methanol/water in order to optimize the electrospray solvent for polarity switching MSI.

The IR-MALDESI imaging source was fully synchronized with a Q Exactive Plus (Thermo Fisher Scientific, Bremen, Germany) mass spectrometer such that laser desorption and ion acquisition events were coordinated at each voxel. Due to the pulsed nature of IR-MALDESI, the automatic gain control (AGC) is turned off for imaging experiments. AGC uses a pre-scan to ensure a consistent number of ions are sampled per spectrum and space charge effects are minimized. When AGC is turned off, ions are accumulated into the C-trap for a fixed injection time (IT), and parts per million (ppm) mass accuracy can be achieved by using lock mass calibrants.⁴⁷ The peaks of diisooctyl phthalate at 391.28429 [M+H]⁺ and

1
2
3 413.26623 [M+Na]⁺ were used as lock masses in positive-ion mode, and peaks of palmitic acid at
4
5 255.2329 [M-H]⁻ and stearic acid at 283.2643 [M-H]⁻ were used as lock masses in negative-ion mode.
6
7

8 Two laser pulses ($f_{\text{rep}} = 20$ Hz) per voxel were used to facilitate complete and reproducible
9
10 desorption of material from the tissue. Ions generated by both laser pulses were accumulated into the
11
12 C-trap for a fixed injection time (IT = 110 ms), and measured in a single Orbitrap acquisition. An
13
14 instrument acquisition method was created using the accompanied software (Xcalibur, Thermo Fisher
15
16 Scientific, Bremen, Germany) to acquire full MS spectra with alternating polarities at each voxel (**Fig.**
17
18 **1A**). A delay was incorporated into the method using the IR-MALDESI control software, where the signal
19
20 for laser desorption and the subsequent signal acquisition by MS was delayed by 96 ms in order to allow
21
22 the electrospray to stabilize upon polarity switching. At each voxel the m/z range of 250-1000 was
23
24 measured with the resolving power of 140,000 (FWHM, $m/z=200$). The focal diameter of the laser was
25
26 ~ 300 μm on burn paper (Zap-It Corporation, Salisbury, NH, USA); however, the desorption diameter
27
28 (spot size) on tissue was measured to be 150 μm .¹⁸ Spatial resolution of 100 μm was achieved by using
29
30 the oversampling method.⁴⁸
31
32
33
34

35 *Data Analysis and Metabolite Identification*

36

37
38 The raw files generated by the Q Exactive Plus instrument for each tissue section were
39
40 converted to mzML format using the msConvert tool from ProteoWizard.⁴⁹ Each mzML file was then
41
42 converted to imzML format⁵⁰ using the imzML converter program⁵¹, and the imzML files were then
43
44 combined into one imzML file using the imzML converter.⁵¹ This file was subsequently loaded into
45
46 MSiReader⁵², a free and open-source software developed for processing high resolving power MSI data,
47
48 by selecting the desired ionization mode (positive or negative). All images were generated using a bin
49
50 width of 5 ppm, without any normalization or interpolation. Centroid values for determining MMA of
51
52 analytes in each ionization mode (Electronic Supplementary Information, **Fig. S1** and **Fig. S2**) were
53
54 obtained using RawMeat, version 2.1 (VAST Scientific, Cambridge, MA, USA). Box-and-whisker plots of
55
56
57
58
59
60

1
2
3 tissue-specific ion abundances (**Fig. S3**) were generated using JMP Pro, version 12 (SAS Institute, Cary,
4
5
6 NC, USA).
7

8 The built-in peak picking tool in MSiReader was used to extract peaks based on spatial
9
10 distribution and changes in ion abundance between the two tissues. Using this function, the software
11
12 averages the spectra over a region of interest specified by the user, and identifies peaks that exhibit
13
14 unique distribution or pronounced changes in ion abundance relative to a user-specified reference
15
16 region. Unique ions must be present in >80% of interrogated region with respect to a reference region,
17
18 and have an average abundance ratio greater than 2. The generated peak lists were searched against
19
20 databases such as METLIN⁵³ and LIPID MAPS⁵⁴, and putative compound identification was made possible
21
22 by using the accurate mass in tandem with fundamental mass spectrometry concepts such as spectral
23
24 accuracy^{55,56} and sulfur counting.^{57,58}
25
26
27

28 **Results and Discussion**

29 *Polarity Switching MSI Method Development*

30
31 Applications of polarity switching in MSI analyses have emerged recently, with most reports
32
33 using MALDI as the ionization mode.⁵⁹⁻⁶¹ Due to limitations of MALDI MSI, some of which were
34
35 mentioned above, polarity switching IR-MALDESI MSI of tissue sections at atmospheric pressure is of
36
37 interest. As shown in **Figure 1A**, the IR-MALDESI polarity switching method was developed such that
38
39 adjacent voxels are analyzed with opposite polarities. In addition, a delay of 96 ms was incorporated
40
41 after each polarity switching event to allow the electrospray to stabilize before sampling the subsequent
42
43 voxel. This pattern is repeated across the area of the tissue, and data is parsed and analyzed according
44
45 to the polarity. One of the advantages of this polarity switching method is shortening the data
46
47 acquisition time drastically. In order to obtain the same biochemical information two MSI experiments,
48
49 one in each ionization mode, could be performed, and the amount of time, in milliseconds, required to
50
51 analyze the tissue sections in both modes can be calculated as $T = 1244x$, where x is the number of
52
53
54
55
56
57
58
59
60

1
2
3 voxels. However, using the polarity switching MSI method developed in this work, the data acquisition
4
5 time can be calculated as $T = 718x$, after accounting for the 96 ms delay after each polarity switching
6
7 event. Therefore, the polarity switching method reduces the data acquisition time by 42%, while
8
9 providing the same biochemical information. In addition, since all measurements are made from the
10
11 same tissue section, sample preparation times are also reduced.
12
13

14
15 It is worth noting that parsing the data based on polarity will result in ion images with an
16
17 increased resolution in the X dimension (horizontal) by a factor of two; however, the resolution in the Y
18
19 dimension (vertical) remains the same (**Fig. 1B**). Since screening the distribution of hundreds of analytes
20
21 is the objective in untargeted polarity switching MSI analyses, this loss in spatial resolution in the X
22
23 dimension will not likely affect the depth of spectral information obtained. Once a list of candidates for
24
25 targeted analyses has been generated, MSI at higher resolutions can be performed.
26
27

28
29 One of concerns when performing polarity switching experiments is that switching the polarity
30
31 will deteriorate the mass accuracy due to temporarily unstable operation of electronics in the
32
33 instrument. Schuhmann *et al.* reported a degradation of mass accuracy upon successive polarity
34
35 switching in shotgun analysis of lipids; however, they showed that using AGC and lock mass calibration
36
37 will help preserve mass accuracy.⁶² Since IR-MALDESI MSI analyses are performed with AGC off, the
38
39 mass measurement accuracy (MMA) of two representative ions, cholesterol in positive-ion mode and
40
41 glutathione in negative-ion mode, are presented for all scans across both healthy and cancerous tissue
42
43 sections (**Fig. S1** and **Fig. S2**, respectively), in order to ensure high mass accuracy was preserved
44
45 throughout the experiments. The mass accuracy of all putatively identified analytes exhibited the same
46
47 relatively normal distribution, with no biases toward analytes at high or low m/z range. It was confirmed
48
49 that using lock mass calibration alone with AGC turned off, resulted in preserving high mass accuracy
50
51 (MMA ≤ 2.5 ppm) for the duration of analysis time (>4 hours) even with a dynamic number of ions
52
53 sampled during an imaging experiment.
54
55
56
57
58
59
60

Polarity Switching MSI Solvent Optimization

1
2
3
4
5
6
7
8
9
10
11
12
13
14
15
16
17
18
19
20
21
22
23
24
25
26
27
28
29
30
31
32
33
34
35
36
37
38
39
40
41
42
43
44
45
46
47
48
49
50
51
52
53
54
55
56
57
58
59
60

In contrast to MALDI MSI where the choice of matrix depends on the analyte(s) and the ionization mode⁶³, the ice matrix in IR-MALDESI MSI can be used universally for analysis of compounds in either positive- or negative-ion modes without imposing any further restrictions on the size of the analytes. This is due to the fact that IR-MALDESI analyses do not rely on efficient extraction of analytes into the matrix crystals, and the ice matrix is solely used to facilitate the desorption of neutral materials from the tissue surface. Therefore, there is no need for optimizing the matrix used. Nevertheless, a crucial step in IR-MALDESI MSI is partitioning of the neutral tissue-related materials into the charged droplets of the orthogonal electrospray. The geometry of the source along with the electrospray solvent composition for positive ionization mode were previously optimized using a statistical design of experiments (DOE).¹⁸ However, in order to improve ion abundance in both polarities and achieve the most comprehensive coverage of lipids and metabolites in both polarities, the electrospray solvent composition was optimized for polarity switching MSI.

A mouse liver tissue, representing a “homogeneous” tissue at the spatial resolution of these experiments, was used to investigate the effects of adding different modifiers such as weak acids, salts, and other bases to the electrospray solvent for a polarity switching experiment. Four modifiers (ammonium hydroxide, ammonium acetate, acetic acid, and TFE) were chosen based on literature review^{61,62,64}, and added to the electrospray solvent (50:50 MeOH/H₂O) at varying concentrations. The mouse liver tissue section was analyzed in quadrants, where each quadrant was imaged using a specific modifier (**Fig. 2**). The resulting ion images were then combined in order to reconstruct the original tissue shape and perform side-by-side comparison. The tissue-related peaks in each quadrant along with their average ion abundances were extracted using MSiReader. A total of 583 tissue-specific ions (478 in +ESI, 105 in –ESI) were identified using this method. All tissue-related ions were present in each quadrant;

1
2
3 however, their abundance varied from one quadrant to another. Representative ion images of the liver
4 tissue with four modifiers are shown in **Fig. 2**. Upon visual inspection of ion images, it appeared that
5 images generated using acetic acid as the modifier exhibited the highest ion abundance. In order to test
6 this hypothesis, analysis of variance (ANOVA) was performed on datasets obtained in positive- and
7 negative-ion modes, and it was determined that acetic acid and TFE resulted in a significant increase of
8 ion abundance in both ionization modes compared to ammonium hydroxide and ammonium acetate.
9 Since the abundance of ions generated using acetic acid and TFE were not significantly different from
10 each other, additional criteria such as difference in ion abundance between the two ionization modes,
11 total ion current (TIC) stability throughout the experiment, and %RSD per voxel were taken into account.
12 In order to ensure there was no systematic bias for one ionization mode over the other, box-and-
13 whisker plots of abundance of tissue-specific ions in both modes were generated. These plots for acetic
14 acid are presented in **Fig. S3**, and confirm that the sensitivity in both ionization modes were comparable
15 and no bias was observed. Based on these additional criteria, 1 mM acetic acid was chosen as optimum
16 modifier added to the electrospray solvent for polarity switching.

Polarity Switching MSI of Healthy and Cancerous Tissue Sections

17
18
19
20
21
22
23
24
25
26
27
28
29
30
31
32
33
34
35
36
37
38
39
40
41
42
43
44
45
46
47
48
49
50
51
52
53
54
55
56
57
58
59
60
Healthy and cancerous hen ovarian tissue sections were analyzed using the developed polarity
switching method and optimized electrospray solvent. The obtained images were analyzed side-by-side,
and tissue-specific ions were extracted using MSiReader. Differences in spatial distribution and relative
abundance of analytes between the two tissue sections could be readily discerned. Representative
images demonstrating these differences are shown in **Fig 3A**, and the location of follicles in healthy and
cancerous tissue section are denoted with dashed or straight lines, respectively. It can be seen that
cholesterol (m/z 369.3516, $[M-H_2O+H]^+$) is relatively homogeneously distributed across the healthy
tissue section; whereas, putatively assigned 16:3-Glc-Campesterol (m/z 795.6106, $[M+H]^+$) is more
abundant in one of the follicles of this tissue section. The differences in the relative abundance between

1
2
3 the two tissues is of more importance, and could provide molecular insight into the underlying biology.
4
5 It can be seen that cholesterol, PS (18:4) (m/z 518.2504, $[M+H]^+$), glutathione (m/z 306.0763, $[M-H]^-$),
6
7 and PI (38:4) (m/z 885.5501, $[M-H]^-$) are present at a higher abundance in the cancerous tissue section.
8
9 Conversely, putatively assigned α -tocopherol (m/z 429.3739, $[M-H]^+$) is more abundant in the healthy
10
11 tissue section. These observations are in good agreement with those reported in the literature obtained
12
13 using conventional methods.^{21,42,65} In order to ensure a comprehensive lipid data across different classes
14
15 was obtained, mass excess⁶⁶ of tissue-specific ions for each tissue section were overlaid on mass excess
16
17 distribution of all lipid classes obtained from LIPID MAPS database⁵⁴, and it was shown that the majority
18
19 of identified ions belong to lipids from various classes in the m/z range measured (**Fig. 3B**). Additionally,
20
21 an approximate 2-fold increase in the number of lipids identified in the cancerous tissue was observed.
22
23 Lipid classes such as fatty acids, phospholipids, and sphingolipids accounted for most of the difference in
24
25 the number of identified lipids between the two tissue sections.
26
27
28
29
30

31 As mentioned in experimental section, metabolites and lipids were identified by searching their
32
33 accurate mass against METLIN⁵³ and LIPID MAPS⁵⁴ databases. In many cases where more than one
34
35 metabolite corresponded to the same accurate mass, fundamental mass spectrometry concepts such as
36
37 spectral accuracy⁵⁵ and sulfur counting⁵⁶ were used to distinguish and validate the identity of an analyte.
38
39 The ion detected at m/z 306.0766 in negative-ion mode was used as an example to demonstrate this
40
41 process, since the images obtained for this ion (**Fig. 3A**) exhibited an 8-fold increase in relative
42
43 abundance in the cancerous tissue. A METLIN database search for this ion using a 5 ppm window results
44
45 in four molecules, three of which are isomers, that could potentially represent the ion detected (**Fig.**
46
47
48
49
50
51
52
53
54
55
56
57
58
59
60
4A). The relative abundance of M+1 peak can be used to calculate the number of carbons present in the
molecule, and identify the compound as glutathione (**Fig. 4B**). Further confirmation can be achieved by
inspecting the M+2 peaks from high resolving power MS and their abundance relative to the
monoisotopic peak in order to investigate the presence of atoms such as chlorine and sulfur. The natural

1
2
3 abundance of ^{34}S is 3.976%-4.734% as reported by the International Union of Pure and Applied
4 Chemistry (IUPAC)⁶⁷, therefore the relative abundance of M+2 in the inset of **Fig. 4B** confirms the
5
6 presence of 1 sulfur atom in the observed ion. These isotopic abundance patterns have been shown to
7
8 be more powerful for identifying metabolites compared to mass measurement accuracy of <1 ppm
9
10 alone.⁶⁸ It is important to remember that utilizing these concepts will require employing of high
11
12 resolving power instruments. This is especially the case for MSI experiments, since they entail direct
13
14 analysis of samples from surfaces and chromatographic separations are not used to reduce the
15
16 complexity of spectra. For instance, a resolving power of >40,000 is required to resolve the $^{34}\text{S}_1$ peak
17
18 from $^{18}\text{O}_1$ and $^{13}\text{C}_2$ peaks in glutathione (**Fig. 4B**). It is worth noting that spectral accuracy cannot
19
20 distinguish between isomers, which demands the use of tandem MS.
21
22
23
24
25

26
27 As noted, images presented in **Fig. 3A** are only a small representative of the differences
28
29 observed in lipid content of the two tissue section. In order to demonstrate the scale of data generated,
30
31 the spectra from both healthy and cancerous tissue sections are shown in **Fig 5**. The complexity of each
32
33 set of spectra highlights the need for high resolving power instrumentation in ambient MSI applications,
34
35 and signifies the importance of polarity switching for extensive investigation of metabolites and lipids in
36
37 tissue sections. Additionally, the number of peaks observed and their relative abundance vary
38
39 significantly between the cancerous and healthy tissue sections. The m/z range of 250-400, mostly
40
41 consisting of fatty acids, and the m/z range of 500-850, mostly dominated by phospholipids, sterols, and
42
43 sphingolipids are two regions that stand out the most. Elevation in levels of these lipid classes are one of
44
45 the most common alterations observed in cancerous cells.^{21,42,69} Fatty acids are fundamental building
46
47 blocks of complex lipids, and are involved in energy storage and membrane proliferation. Elevated levels
48
49 of fatty acids in many different cancerous cells, including ovarian cancer cells, have been reported.^{43-45,70}
50
51 This increase can be attributed to an increase in the *de novo* biosynthesis or an increase in the rate of
52
53 uptake of these lipids from the surrounding environment.^{44,70} These fatty acids can then be stored in
54
55
56
57
58
59
60

1
2
3 lipid droplets to provide necessary energy for rapid proliferation, or they can be incorporated in the
4
5 synthesis of more complex lipids such as phospholipids. Sterols and different classes of phospholipids
6
7 are key structural lipids in cell membranes. There have been numerous reports of elevated levels of
8
9 these lipid classes in cancerous cells, in order to build new membranes and maintain active
10
11 signaling.^{21,71,72} Another class of lipids occupying this *m/z* range are sphingolipids. These lipids, especially
12
13 ceramides and sphingomyelins, are bioactive lipids that function as effector molecules and have
14
15 important roles in stimulus-mediated signaling and regulation such as growth, inhibition, and
16
17 apoptosis.⁶⁹ Several reports indicate that these lipids are present at higher levels in cancer cells,
18
19 presumably in order to increase signaling of cell growth receptors and facilitate rapid growth and
20
21 proliferation of cancerous cells.^{69,73}
22
23
24
25

26
27 The high degree of agreement between these observations and those obtained using
28
29 conventional methods confirms the utility of polarity switching IR-MALDESI MSI for screening changes in
30
31 lipid metabolism in cancer cells by simultaneously monitoring the relative abundance of hundreds of
32
33 metabolites and lipids, as well as their spatial distribution within tissue sections. Current studies are
34
35 focused on applying this method to analyze tissues from a biorepository generated in our laboratory,
36
37 which contains healthy tissues, as well as cancerous tissues at different stages (I-IV) from 150 hens.
38
39 Furthermore, the lipid and metabolite data obtained using polarity switching MSI will be paired with
40
41 proteomics information²⁶ obtained from serial tissue sections in order to gain insight into metabolic
42
43 pathways altered in ovarian cancer.
44
45
46

47 **Conclusions**

48
49 This work demonstrates the development of a polarity switching IR-MALDESI MSI method for
50
51 screening the spatial distribution and relative abundance of different metabolites and lipids in healthy
52
53 and cancerous tissues. The electrospray solvent was optimized for these analyses in order to obtain a
54
55 comprehensive metabolite and lipid data, and fundamental mass spectrometry concepts were used to
56
57
58
59
60

1
2
3 identify the analytes after database searching. Lipid classes such as fatty acids, phospholipids, and
4
5 sphingolipids exhibited significantly higher relative abundances in cancerous tissue compared to the
6
7 healthy tissue. These results indicate the potential of polarity switching IR-MALDESI MSI in discovery of
8
9 biomarkers for ovarian cancer.
10

11 **Acknowledgments**

12
13 The authors would like to thank Prof. Troy Ghashghaei from NCSU Department of Molecular Biomedical
14
15 Sciences and Prof. James Petite from NCSU Department of Poultry Science for providing the mouse liver
16
17 and hen ovary tissues, respectively. The authors also gratefully acknowledge financial assistance
18
19 received from the National Institutes of Health (R01GM087964), the W. M. Keck foundation, and North
20
21 Carolina State University.
22
23
24
25

26 **Notes and References**

- 27
28
29
30 1 J. B. Fenn, M. Mann, C. K. Meng, S. F. Wong and C. M. Whitehouse, *Science*, 1989, **246**, 64–71.
31
32 2 M. Karas and F. Hillenkamp, *Anal. Chem.*, 1988, **60**, 2299–2301.
33
34 3 K. Tanaka, H. Waki, Y. Ido, S. Akita and Y. Yoshida, *Rapid Commun. Mass Spectrom.*, 1988, **2**, 151–
35
36 153.
37
38 4 R. Aebersold and M. Mann, *Nature*, 2003, **422**, 198–207.
39
40 5 J. D. Wulfkühle, L. A. Liotta and E. F. Petricoin, *Nat. Rev. Cancer*, 2003, **3**, 267–275.
41
42 6 E. P. Diamandis, *Mol. Cell. Proteomics*, 2004, **3**, 367–378.
43
44 7 D. E. van der Merwe, K. Oikonomopoulou, J. Marshall and E. P. Diamandis, *Adv. Cancer Res.*,
45
46 2006, **96**, 23–50.
47
48 8 L. A. McDonnell, G. L. Corthals, S. M. Willems, A. van Remoortere, R. J. M. van Zeijl and A. M.
49
50 Deelder, *J. Proteomics*, 2010, **73**, 1921–1944.
51
52 9 L. S. Eberlin, A. L. Dill, A. B. Costa, D. R. Iffa, L. Cheng, T. Masterson, M. Koch, T. L. Ratliff and R. G.
53
54 Cooks, *Anal. Chem.*, 2010, **82**, 3430–3434.
55
56 10 L. S. Eberlin, I. Norton, A. L. Dill, A. J. Golby, K. L. Ligon, S. Santagata, R. Graham Cooks and N. Y. R.
57
58 Agar, *Cancer Res.*, 2012, **72**, 645–654.
59
60

- 1
2
3
4 11 C. Schöne, H. Höfler and A. Walch, *Clin. Biochem.*, 2013, **46**, 539–545.
5
6 12 S. A. Schwartz, M. L. Reyzer and R. M. Caprioli, *J. mass Spectrom.*, 2003, **38**, 699–708.
7
8 13 P. Chaurand, D. S. Cornett, P. M. Angel and R. M. Caprioli, *Mol. Cell. proteomics*, 2011, **10**,
9 O110.004259.
10
11 14 V. V Laiko, M. A. Baldwin and A. L. Burlingame, *Anal. Chem.*, 2000, **72**, 652–7.
12
13
14 15 Z. Takáts, J. M. Wiseman, B. Gologan and R. G. Cooks, *Science*, 2004, **306**, 471–473.
15
16 16 J. S. Sampson, A. M. Hawkrige and D. C. Muddiman, *J. Am. Soc. Mass Spectrom.*, 2006, **17**,
17 1712–1716.
18
19 17 G. Robichaud, J. A. Barry and D. C. Muddiman, *Encycl. Anal. Chem.*, 2014.
20
21 18 G. Robichaud, J. A. Barry and D. C. Muddiman, *J. Am. Soc. Mass Spectrom.*, 2014, **25**, 319–328.
22
23 19 E. P. Rosen, M. T. Bokhart, H. T. Ghashghaei and D. C. Muddiman, *J. Am. Soc. Mass Spectrom.*,
24 2015, **26**, 899–910.
25
26 20 M. R. Wenk, *Nat. Rev. Drug Discov.*, 2005, **4**, 594–610.
27
28 21 C. R. Santos and A. Schulze, *FEBS J.*, 2012, **279**, 2610–2623.
29
30 22 I. J. Goldberg, C. M. Trent and P. C. Schulze, *Cell Metab.*, 2012, **15**, 805–812.
31
32 23 M. Pulfer and R. C. Murphy, *Mass Spectrom. Rev.*, 2003, **22**, 332–64.
33
34 24 R. B. Dixon, M. S. Bereman, J. N. Petite, A. M. Hawkrige and D. C. Muddiman, *Int. J. Mass*
35 *Spectrom.*, 2011, **305**, 79–86.
36
37 25 G. L. Andrews Kingon, J. N. Petite, D. C. Muddiman and A. M. Hawkrige, *Methods*, 2013, **61**,
38 323–30.
39
40 26 A. I. Nepomuceno, H. Shao, K. Jing, Y. Ma, J. N. Petite, M. O. Idowu, D. C. Muddiman, X. Fang and
41 A. M. Hawkrige, *Anal. Bioanal. Chem.*, 2015.
42
43 27 R. Siegel, J. Ma, Z. Zou and A. Jemal, *CA Cancer J. Clin.*, 2014, **64**, 9–29.
44
45 28 K. a. Lowe, V. M. Chia, A. Taylor, C. O'Malley, M. Kelsh, M. Mohamed, F. S. Mowat and B. Goff,
46 *Gynecol. Oncol.*, 2013, **130**, 107–114.
47
48 29 Z. Yurkovetsky, S. Skates, A. Lomakin, B. Nolen, T. Pulsipher, F. Modugno, J. Marks, A. Godwin, E.
49 Gorelik, I. Jacobs, U. Menon, K. Lu, D. Badgwell, R. C. Bast and A. E. Lokshin, *J. Clin. Oncol.*, 2010,
50 **28**, 2159–2166.
51
52
53
54
55
56
57
58
59
60

- 1
2
3 30 U. Menon, M. Griffin and A. Gentry-Maharaj, *Gynecol. Oncol.*, 2014, **132**, 490–5.
4
5
6 31 P. A. Johnson and J. R. Giles, *Nat. Rev. Cancer*, 2013, **13**, 432–436.
7
8 32 L. K. Mullany and J. S. Richards, *Endocrinology*, 2012, **153**, 1585–1592.
9
10 33 S. L. Stewart, T. D. Querec, A. R. Ochman, B. N. Gruver, R. Bao, J. S. Babb, T. S. Wong, T.
11 Koutroukides, A. D. Pinnola, A. Klein-Szanto, T. C. Hamilton and C. Patriotis, *Cancer Res.*, 2004, **64**,
12 8177–8183.
13
14
15 34 A. M. Hawkrigde, *Proteomics Clin. Appl.*, 2014, **8**, 689–699.
16
17 35 E. Lengyel, J. E. Burdette, H. a Kenny, D. Matei, J. Pilrose, P. Haluska, K. P. Nephew, D. B. Hales
18 and M. S. Stack, *Oncogene*, 2014, **33**, 3619–3633.
19
20
21 36 A. Barua, P. Bitterman, J. S. Abramowicz, A. L. Dirks, J. M. Bahr, D. B. Hales, M. J. Bradaric, S. L.
22 Edassery, J. Rotmensch and J. L. Luborsky, *Int. J. Gynecol. cancer*, 2009, **19**, 531–539.
23
24 37 L. S. Treviño, E. L. Buckles and P. A. Johnson, *Cancer Prev. Res.*, 2012, **5**, 343–349.
25
26
27 38 R. Lemaire, S. A. Menguellat, J. Stauber, V. Marchaudon, J. Lucot, P. Collinet, M. Farine, D.
28 Vinatier, R. Day, P. Ducoroy, O. M. Salzet and I. Fournier, *J. Poteome Res.*, 2007, **6**, 4127–4134.
29
30 39 L. H. Cazares, D. Troyer, S. Mendrinos, R. A. Lance, J. O. Nyalwidhe, H. A. Beydoun, M. A.
31 Clements, R. R. Drake and O. J. Semmes, *Clin. Cancer Res.*, 2009, **15**, 5541–51.
32
33
34 40 J. O. R. Gustafsson, M. K. Oehler, A. Ruzskiewicz, S. R. McColl and P. Hoffmann, *Int. J. Mol. Sci.*,
35 2011, **12**, 773–94.
36
37 41 S. Meding, K. Martin, O. J. R. Gustafsson, J. S. Eddes, S. Hack, M. K. Oehler and P. Hoffmann, *J.*
38 *Proteome Res.*, 2013, **12**, 308–15.
39
40 42 J. A. Menendez and R. Lupu, *Nat. Rev. Cancer*, 2007, **7**, 763–777.
41
42
43 43 M. Tania, M. A. Khan and Y. Song, *Curr. Oncol.*, 2010, **17**, 6–11.
44
45 44 K. M. Nieman, H. A. Kenny, C. V Penicka, A. Ladanyi, R. Buell-Gutbrod, M. R. Zillhardt, I. L.
46 Romero, M. S. Carey, G. B. Mills, G. S. Hotamisligil, S. D. Yamada, M. E. Peter, K. Gwin and E.
47 Lengyel, *Nat. Med.*, 2011, **17**, 1498–503.
48
49
50 45 N. Zaidi, L. Lupien, N. B. Kuemmerle, W. B. Kinlaw, J. V. Swinnen and K. Smans, *Prog. Lipid Res.*,
51 2013, **52**, 585–589.
52
53
54 46 G. Robichaud, J. A. Barry, K. P. Garrard and D. C. Muddiman, *J. Am. Soc. Mass Spectrom.*, 2013,
55 **24**, 92–100.
56
57
58
59
60

- 1
2
3 47 J. V Olsen, L. M. F. de Godoy, G. Li, B. Macek, P. Mortensen, R. Pesch, A. Makarov, O. Lange, S.
4 Horning and M. Mann, *Mol. Cell. Proteomics*, 2005, **4**, 2010–21.
5
6
7 48 J. C. Jurchen, S. S. Rubakhin and J. V Sweedler, *J. Am. Soc. Mass Spectrom.*, 2005, **16**, 1654–9.
8
9 49 D. Kessner, M. Chambers, R. Burke, D. Agus and P. Mallick, *Bioinformatics*, 2008, **24**, 2534–6.
10
11 50 T. Schramm, A. Hester, I. Klinkert, J. P. Both, R. M. A. Heeren, A. Brunelle, O. Lapr evote, N.
12 Desbenoit, M. F. Robbe, M. Stoeckli, B. Spengler and A. R ompp, *J. Proteomics*, 2012, **75**, 5106–
13 5110.
14
15
16 51 A. M. Race, I. B. Styles and J. Bunch, *J. Proteomics*, 2012, **75**, 5111–5112.
17
18 52 G. Robichaud, K. P. Garrard, J. A. Barry and D. C. Muddiman, *J. Am. Soc. Mass Spectrom.*, 2013,
19 **24**, 718–721.
20
21 53 C. A. Smith, G. O’Maille, E. J. Want, C. Qin, S. A. Trauger, T. R. Brandon, D. E. Custodio, R. Abagyan
22 and G. Siuzdak, *Ther. Drug Monit.*, 2005, **27**, 747–51.
23
24
25 54 M. Sud, E. Fahy, D. Cotter, A. Brown, E. A. Dennis, C. K. Glass, A. H. Merrill, R. C. Murphy, C. R. H.
26 Raetz, D. W. Russell and S. Subramaniam, *Nucleic Acids Res.*, 2007, **35**, D527–32.
27
28
29 55 Y. Wang and M. Gu, *Anal. Chem.*, 2010, **82**, 7055–62.
30
31 56 S. L. Blake, S. H. Walker, D. C. Muddiman, D. Hinks and K. R. Beck, *J. Am. Soc. Mass Spectrom.*,
32 2011, **22**, 2269–2275.
33
34 57 S. D. Shi, C. L. Hendrickson and a G. Marshall, *Proc. Natl. Acad. Sci. U. S. A.*, 1998, **95**, 11532–
35 11537.
36
37
38 58 T. R. Hoye, V. Dvornikovs, J. M. Fine, K. R. Anderson, C. S. Jeffrey, D. C. Muddiman, F. Shao, P. W.
39 Sorensen and J. Wang, *J. Org. Chem.*, 2007, **72**, 7544–7550.
40
41
42 59 A. Thomas, J. L. Charbonneau, E. Fournaise and P. Chaurand, *Anal. Chem.*, 2012, **84**, 2048–2054.
43
44 60 A. R. Korte and Y. J. Lee, *J. Am. Soc. Mass Spectrom.*, 2013, **24**, 949–55.
45
46
47 61 C. Janfelt, N. Wellner, H. S. Hansen and S. H. Hansen, *J. Mass Spectrom.*, 2013, **48**, 361–6.
48
49 62 K. Schuhmann, R. Almeida, M. Baumert, R. Herzog, S. R. Bornstein and A. Shevchenko, *J. mass*
50 *Spectrom.*, 2012, **47**, 96–104.
51
52
53 63 R. J. A. Goodwin, *J. Proteomics*, 2012, **75**, 4893–911.
54
55 64 Z. Wu, W. Gao, M. a Phelps, D. Wu, D. D. Miller and J. T. Dalton, *Anal. Chem.*, 2004, **76**, 839–47.
56
57 65 G. K. Balendiran, R. Dabur and D. Fraser, *Cell Biochem. Funct.*, 2004, **22**, 343–352.
58
59
60

- 1
2
3 66 J. L. Frahm, B. E. Howard, S. Heber and D. C. Muddiman, *J. Mass Spectrom.*, 2006, **41**, 281–288.
4
5
6 67 M. Berglund and M. E. Wieser, *Pure Appl. Chem.*, 2011, **83**, 397–410.
7
8 68 T. Kind and O. Fiehn, *BMC Bioinformatics*, 2006, **7**, 234.
9
10 69 B. Ogretmen and Y. A. Hannun, *Nat. Rev. Cancer*, 2004, **4**, 604–616.
11
12 70 E. Currie, A. Schulze, R. Zechner, T. C. Walther and R. V. Farese, *Cell Metab.*, 2013, **18**, 153–161.
13
14 71 E. Ackerstaff, K. Glunde and Z. M. Bhujwala, *J. Cell. Biochem.*, 2003, **90**, 525–533.
15
16 72 L. Gabitova, A. Gorin and I. Astsaturov, *Clin. Cancer Res.*, 2014, **20**, 28–35.
17
18 73 H. Furuya, Y. Shimizu and T. Kawamori, *Cancer Metastasis Rev.*, 2011, **30**, 567–576.
19
20
21
22
23
24
25
26
27
28
29
30
31
32
33
34
35
36
37
38
39
40
41
42
43
44
45
46
47
48
49
50
51
52
53
54
55
56
57
58
59
60

Figures

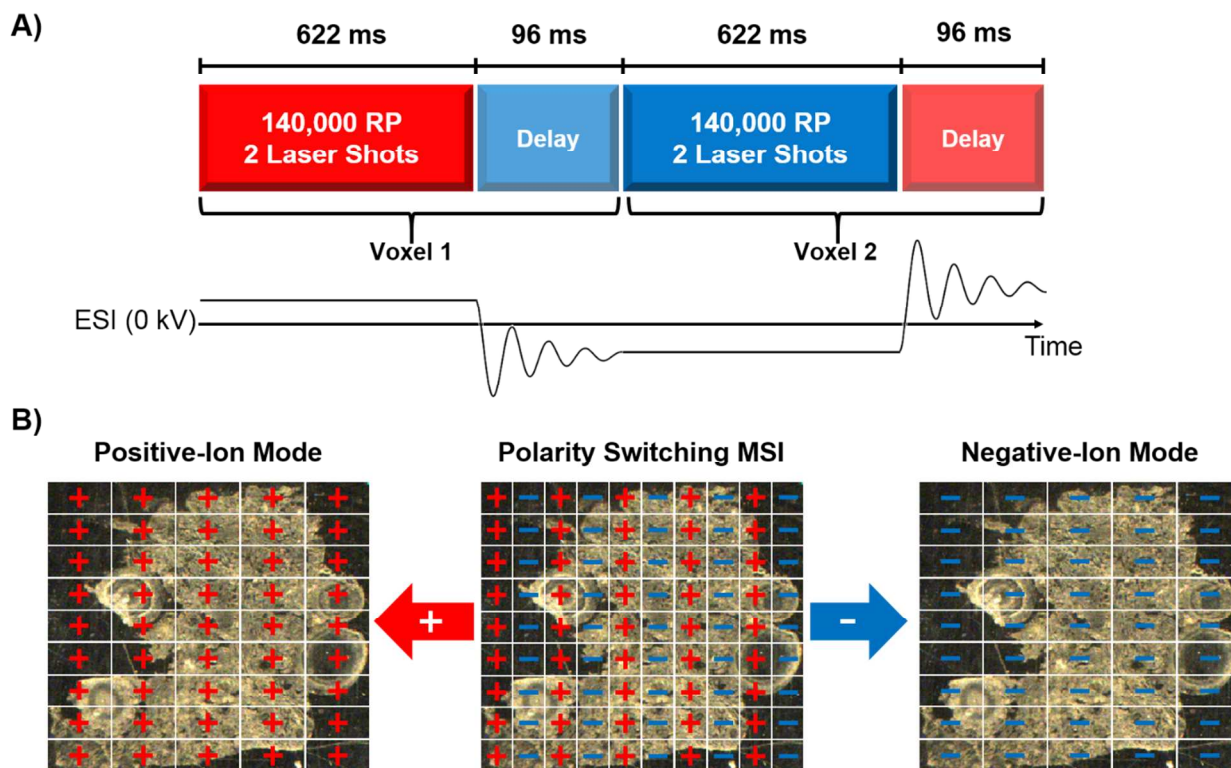


Figure 1. A) Schematic of polarity switching MSI method, where adjacent voxels are analyzed in opposing polarities and a delay incorporated in the method in order to allow the electro spray to stabilize upon switching the polarity. The schematic of electro spray voltage stabilization is shown for demonstration purposes. The stability of electro spray was visually inspected; however, the voltage was not measured. **B)** Representation of polarity switching MSI on tissue sections. Ion images generated for each polarity will have a resolution in the X dimension (horizontal) that is two times larger than in the Y dimension (vertical). The voxels are drawn much larger than actual voxels to aid with visualization of the concept.

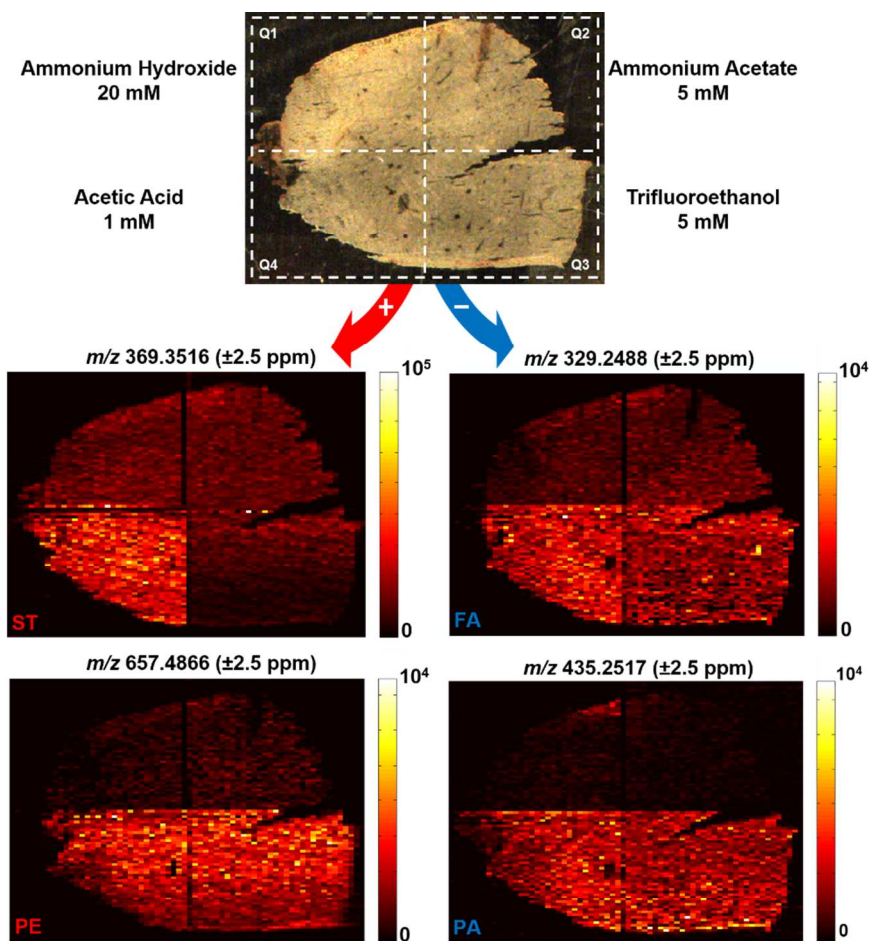


Figure 2. Optical image of the tissue showing the modifiers used in each quadrant, along with representative ion images of lipids in positive- and negative-ion modes, demonstrating different ionization efficiencies in presence of each modifier. The lipid classes, annotated on the bottom left of each image, are as follows: sterol (ST), phosphoethanolamine (PE), fatty acid (FA), phosphatidic acid (PA).

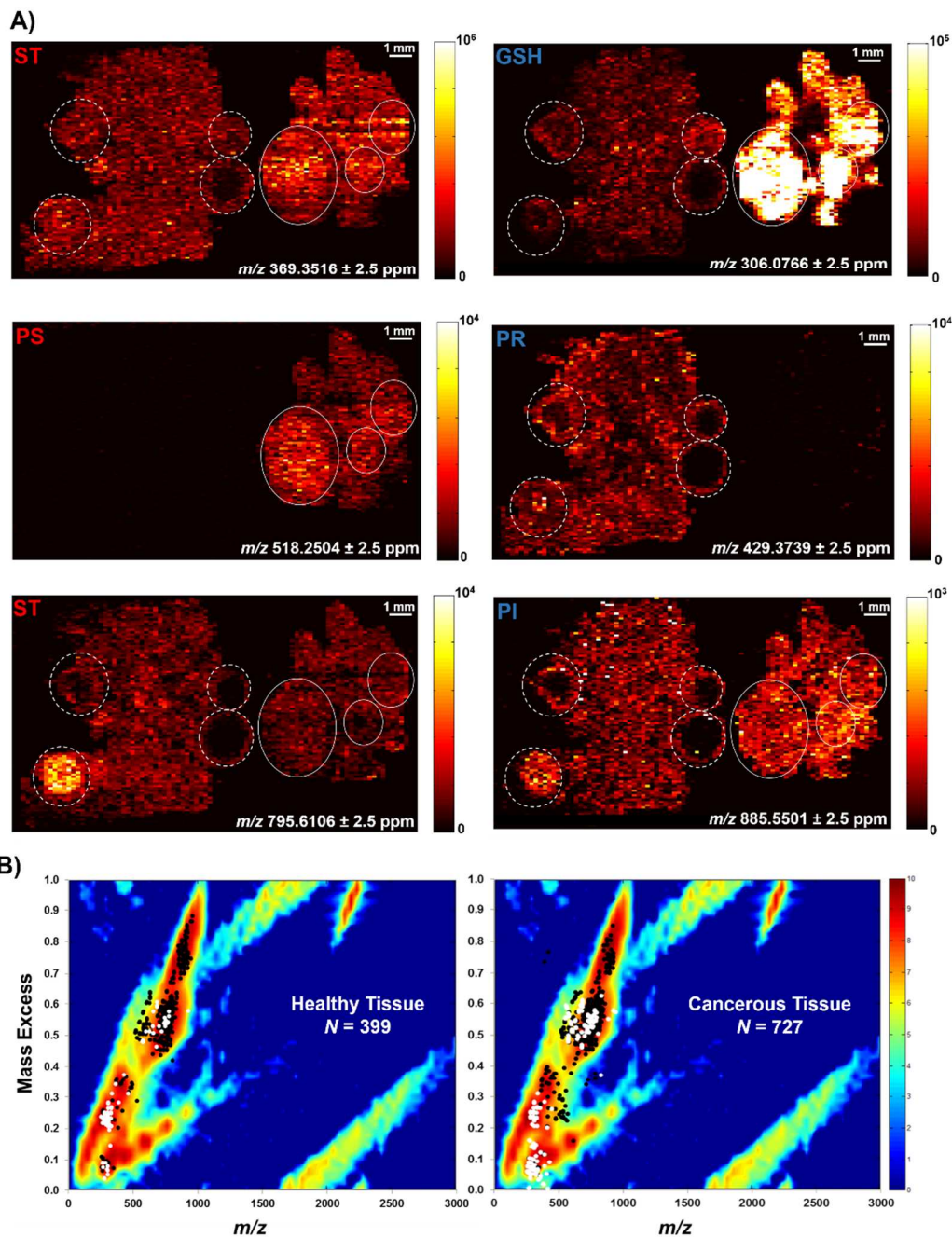


Figure 3. A) Representative ion images of different lipid classes in healthy and cancerous ovarian tissue sections. In each image, the healthy tissue is on the left and the cancerous tissue is on the right, while dashed and solid lines represent the location of follicles in healthy and cancerous tissues, respectively. The metabolite or lipid class in each image, annotated according to the ionization mode that it was detected in, are as follows: sterol (ST), phosphoserine (PS), glutathione (GSH), prenol (PR), and phosphoinositol (PI). **B)** Mass excess of tissue-specific ions overlaid on mass excess distribution of lipids from LIPIDMAPS Database⁵⁴, demonstrating a comprehensive lipid coverage. Black and white dots represent ions detected in positive- and negative-ion modes, respectively.

A)

Compound	Neutral Mass (Da)	MMA (ppm)	Chemical Formula
● Glutathione	307.0838	<1	$C_{10}H_{17}N_3O_6S$
○ Stealthin C	307.0845	<1	$C_{18}H_{13}NO_4$
○ Hallacridone	307.0845	<1	$C_{18}H_{13}NO_4$
○ Aristolodione	307.0845	<1	$C_{18}H_{13}NO_4$

} Isomers

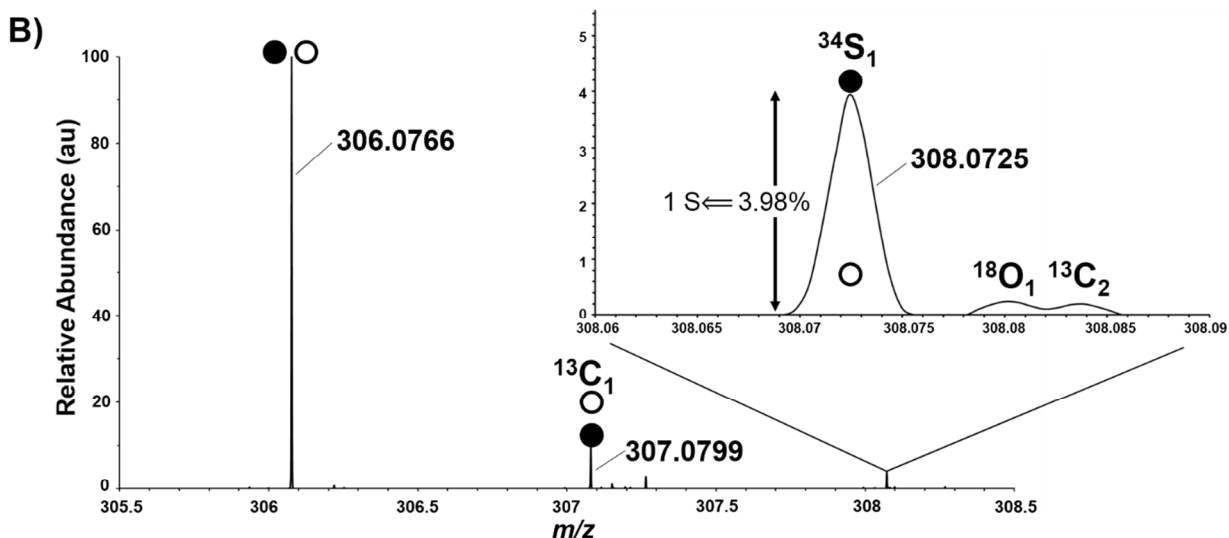


Figure 4. A) Four candidates that could represent the deprotonated species observed at m/z 306.0766 (\pm 2.5 ppm) identified using METLIN database.⁵³ **B)** Confident identification of analyte by utilizing concepts such as spectral accuracy^{55,56} and sulfur counting^{57,58} in tandem with accurate mass to confidently identify an analyte observed in tissue.

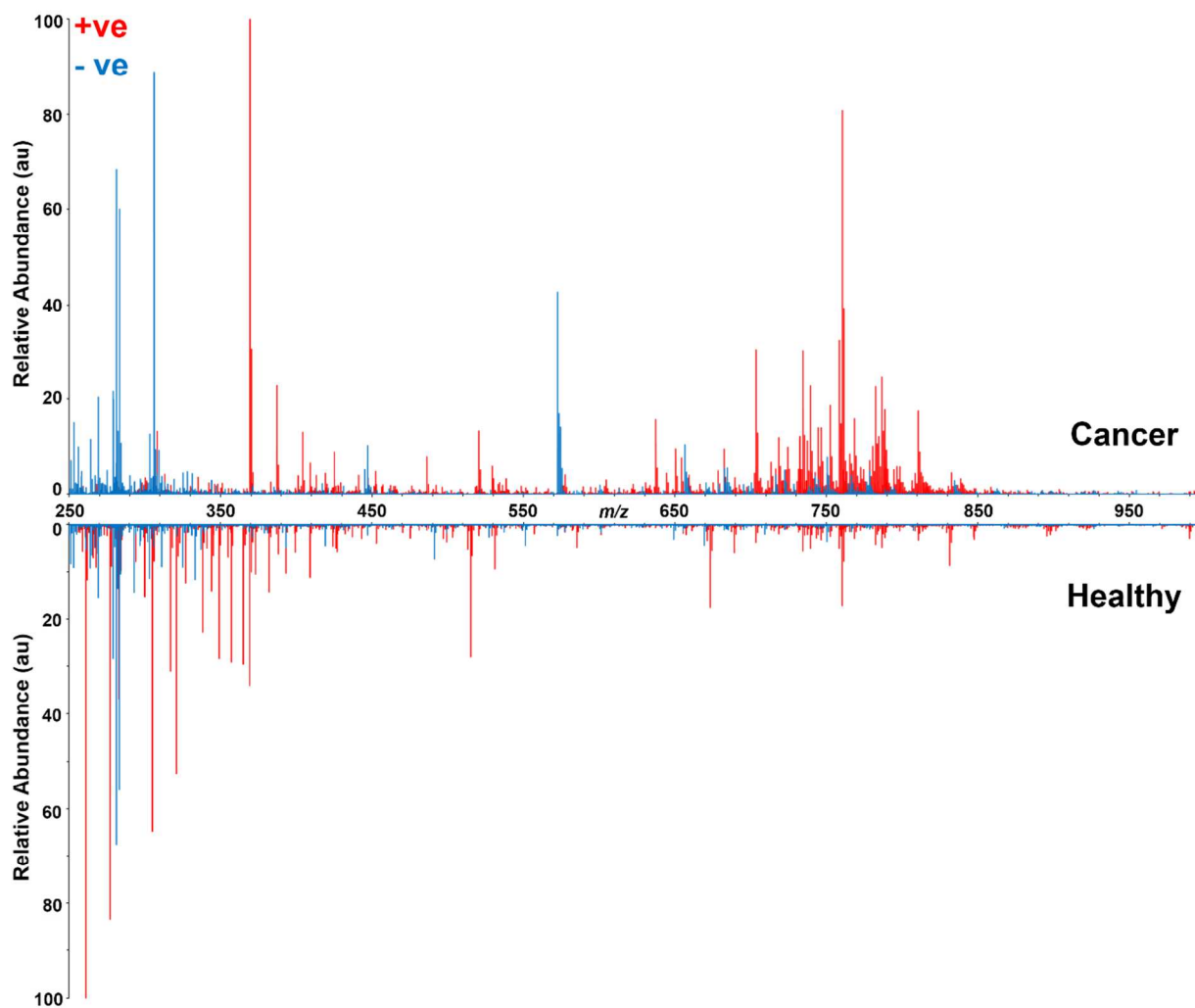


Figure 5. Representative spectra from polarity switching MSI of cancerous (top) and healthy (bottom) tissue sections. The spectra obtained in positive- and negative-ion modes are overlaid and color-coded. It can be seen that lipid classes such as fatty acids (mostly observed in m/z 250-400), phospholipids, sterols, and sphingolipids (often observed in m/z 500-850) are much more abundant in the cancerous tissue compared to the healthy tissue.